Impact of the Combustor-Turbine Interface Slot Orientation on the Durability of a Nozzle Guide Vane Endwall

Alan Thrift
e-mail: alan.thrift@siemens.com

Karen Thole
e-mail: kthole@psu.edu

Mechanical and Nuclear Engineering Department,
Pennsylvania State University,
State College, PA 16803

Satoshi Hada
Mitsubishi Heavy Industries LTD,
Takasago Machinery Works,
Hyogo 676-8686, Japan
e-mail: satoshi_hada@mhi.co.jp

The combustor-turbine interface is an essential component in a gas turbine engine as it allows for thermal expansion between the first stage turbine vanes and combustor section. Although not considered as part of the external cooling scheme, leakage flow from the combustor-turbine interface can be utilized as coolant. This paper reports on the effects of orientation of a two-dimensional leakage slot, simulating the combustor-turbine interface, on the net heat flux reduction to a nozzle guide vane endwall. In addition to adiabatic effectiveness and heat transfer measurements, time-resolved, digital particle image velocimetry (TRDPIV) measurements were performed in the vane stagnation plane. Four interface slot orientations of 90 deg, 65 deg, 45 deg, and 30 deg located at 17% axial chord upstream of a first vane in a linear cascade were studied. Results indicate that reducing the slot angle to 45 deg can provide as much as a 137% reduction to the average heat load experienced by the endwall. Velocity measurements indicate the formation of a large leading edge vortex for coolant injected at 90 deg and 65 deg while coolant injected at 45 deg and 30 deg flows along the endwall and washes up the vane surface at the endwall junction. [DOI: 10.1115/1.4007602]

Introduction

The large range of temperatures experienced by the first stage of the turbine section requires that clearance slots be placed between the combustor and turbine section to allow for thermal expansion. To prevent potentially destructive hot gases from being ingested into these interface slots, the feed cavities are pressurized with relatively cool air bled from the compressor. Although generally overlooked in comparison to film cooling holes, leakage flow from the combustor-turbine interface slot can provide essential cooling to the endwalls of the first stage, nozzle guide vane. A net benefit to engine thermal efficiency can be gained if the performance of the leakage flow in reducing the endwall heat load allows for increased turbine inlet temperatures.

One way to improve the performance of the leakage flow is through the modification of the interface slot orientation. This paper is the first to report the effects of interface slot orientation on the net heat flux reduction experienced by a low pressure, nozzle guide vane endwall in the presence of leakage flow. Thermal measurements are complemented with time-resolved flowfield measurements in the vane stagnation plane. The effects of interface slot orientation are investigated for a high momentum flux ratio typical of that seen in an engine and a low momentum flux ratio as more commonly seen in the literature.

Review of Relevant Literature

Although the combustor-turbine interface slot provides essential cooling to the nozzle guide vane endwall, there is limited research available concerning the geometric parameters influencing the performance of the leakage coolant. Only a few studies have investigated the effects of slot orientation on the performance of leakage coolant.

Y. L. Lin et al. [1] investigated the impact of leakage flow upstream of a nozzle guide vane cascade on the endwall adiabatic effectiveness and passage flowfield. The vane passage had one flat and one axisymmetric contoured endwall with a slope of 45 deg. Both endwalls incorporated a slot that was 90 deg to the inlet flow. Adiabatic effectiveness calculations showed that the effectiveness and coverage of the leakage flow was significantly improved for the leakage slot at a relative angle of 45 deg compared to the leakage slot oriented at 90 deg to the endwall. Leakage flow from both slot angles was shown to reduce endwall secondary flows.

Also utilizing an axisymmetric contoured passage, an experimental study by Rehder and Dannhauer [2] investigated the effects of tangential and perpendicular leakage upstream of a linear, three blade cascade. PIV measurements of the velocity flowfields indicated that injecting coolant tangential to the endwall reduced the strength of the horseshoe vortex (HSV). At higher leakage mass flow rates, the HSV was shown to be nonexistent. In contrast, injecting coolant perpendicular to the endwall strengthened the HSV and increased the size of the passage vortex as the injected coolant promoted the separation of the incoming boundary layer. Secondary losses were shown to increase with perpendicular injection and decrease with tangential injection relative to the zero leakage case. In accordance with the velocity measurements, tangential leakage injection reduced the influence of the secondary flows on the endwall heat transfer. Though similar in peak value, high heat transfer values were shown to penetrate further into the blade passage when coolant was injected perpendicular to the surface as compared to tangential injection.

Incorporating a planar passage, Thrift et al. [3] investigated the effect of leakage slot orientation and location on the stagnation plane flowfield and endwall adiabatic effectiveness in a linear, nozzle guide vane cascade. Adiabatic effectiveness results indicated a significant improvement in local and area averaged effectiveness when the slot orientation was reduced from 90 deg to 45 deg. Time resolved, digital particle image velocimetry measurements in the stagnation plane also showed coolant injected at 90 deg promoted the separation of the incoming boundary layer and resulted in the formation of a large time-averaged vortex. Contrarily, when coolant was injected at 45 deg, no time-averaged vortex was present. One of the only other studies to make

Contributed by the International Gas Turbine Institute (IGTI) of ASME for publication in the JOURNAL OF TURBOMACHINERY. Manuscript received July 16, 2012; final manuscript received August 8, 2012; published online June 5, 2013. Assoc. Editor: David Wisler.

flowfield measurements in the stagnation plane of a vane with coolant injection present was an investigation by Sundaram and Thole [4]. In this study, laser doppler velocimetry (LDV) measurements were performed in the stagnation plane of a nozzle guide vane while incorporating leakage flow from an upstream 45 deg slot as well as an upstream row of film cooling holes inclined at 30 deg. In the presence of film cooling, peak turbulence levels were shown to increase in comparison to the no cooling case. Although the study by Sundaram and Thole [4] did not measure heat transfer, several past studies have indicated that heat transfer is enhanced with an increase in near wall turbulence levels [5–8].

As highlighted from the discussion above, there is sparse data available concerning the effects of interface slot orientation on the resulting endwall cooling performance. This study reports the effects of orientation of an upstream leakage slot on the durability of a vane endwall by providing detailed measurements of adiabatic effectiveness and heat transfer. A net heat flux reduction analysis on the endwall is also performed based on the measurements of adiabatic effectiveness and heat transfer. In addition, flowfield measurements in the stagnation plane of the vane are presented as time-averaged vector fields with contours of turbulence intensity.

Experimental Methods

All thermal and velocity measurements were performed in a low speed, closed loop wind tunnel, depicted in Fig. 1 and previously described by Thrift et al. [3]. Driving the flow through the wind tunnel was a 50 hp fan with a 50 Hz variable frequency drive. After passing through the fan the flow was turned 90 deg before encountering a finned-tubed heat exchanger used to remove the initial heat supplied to the flow by the fan.

After passing through the primary heat exchanger, the flow was turned by another 90 deg elbow before being split into three separate flow paths. A porous plate positioned over the main flow path, diverted some flow to the two outer secondary flow paths to serve as leakage coolant. The flow in each of the secondary flow paths traveled through secondary finned-tube heat exchangers before being passed into respective plenums. The secondary heat exchangers provided additional cooling. Flow was drawn from the upper plenum and into the appropriate leakage coolant plenum on the attached test section using a 2 hp blower. The leakage plenum on the test section supplied coolant to the interface slot. During all experiments the secondary flow was cooled to approximately room temperature at 25 °C.

The freestream temperature that was set depended on the type of thermal measurement being performed. Adiabatic effectiveness and heat transfer measurements were made under steady state conditions with a freestream temperature of approximately 50 °C and 25 °C, respectively. For adiabatic effectiveness experiments, the heated freestream flow and the cooled leakage flow simulated the hot core flow and leakage coolant of the engine with a density ratio of approximately 1.07. Using a temperature difference of approximately 25 °C reduced the measurement uncertainty associated with adiabatic effectiveness. For heat transfer experiments, the temperatures of the freestream and leakage coolant were matched to within 0.25 °C to ensure that the measured endwall heat transfer was solely due to convection.

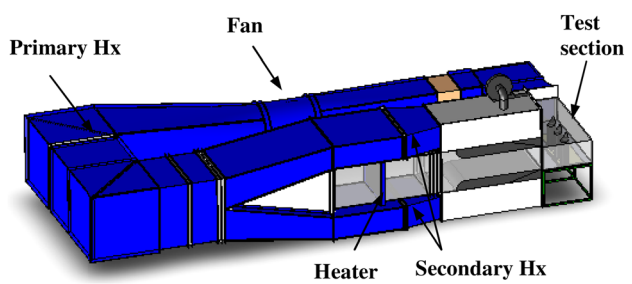

Fig. 1 Depiction of the low speed, closed loop wind tunnel

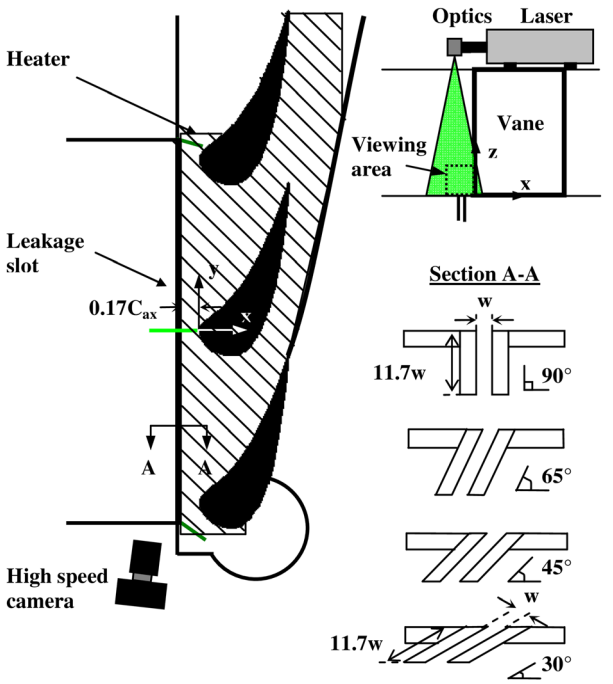

Fig. 2 Schematic of the linear vane cascade with the different leakage slot orientations and the TRDPIV setup

Table 1 Vane geometry and flow conditions

Scaling factor	2.4
Scaled vane chord (C)	46 cm
Axial chord/chord (C_{ax}/C)	0.49
Pitch/chord (P/C)	1.01
Mid span/chord (S/C)	0.6
Inlet, exit Reynolds number (Re_{in}, Re_{exit})	2.0×10^5, 1.0×10^6
Inlet, exit angle (α_{in}, α_{exit})	0 deg, 79 deg
Inlet, exit Mach number (Ma_{in}, Ma_{exit})	0.022, 0.12

Table 2 Inlet turbulent boundary layer characteristics

Boundary layer thickness/mid span (δ/S)	0.34
Displacement thickness/mid span (δ^*/S)	0.038
Momentum thickness/mid span (θ/S)	0.03
Shape factor (δ^*/θ)	1.3
Momentum thickness Reynolds number (Re_θ)	4245

The vane test section was a two-dimensional, linear vane cascade as illustrated in a schematic in Fig. 2. The cascade consisted of two full nozzle guide vanes and a third partial vane connected to a flexible wall. The profile of the flexible wall was adjusted to maintain the desired pressure distribution along the three vanes. The vane design was a spanwise extrusion of a two-dimensional mid span vane geometry. The vanes were scaled up by a factor of 2.4 from engine size to achieve high measurement resolution. A description of the nozzle guide vane parameters and flow conditions is given in Table 1.

The boundary layer entering the cascade was measured at a location 4.25C_{ax} upstream of the vane stagnation by Thrift et al. [9] using the same inlet flow conditions in Table 1. Table 2 lists the turbulent inlet boundary layer parameters, which were maintained throughout this study. The measured turbulence intensity was lower than that typically found in an engine at 1.0%. The

effect of turbulence, however, was not considered in this study as past studies by the authors have evaluated this effect [5].

Leakage flow from the combustor turbine interface was simulated using a two-dimensional slot placed on the bottom endwall, upstream of the vane stagnation as illustrated in Fig. 2. To investigate the effects of slot orientation, experiments were performed with orientations of 90 deg, 65 deg, 45 deg, and 30 deg. As indicated in Fig. 2, each slot had a flow length-to-width of 11.7. Also note that the downstream edge of each slot was located at $x = -0.17C_{ax}$ from the vane stagnation.

The mainstream conditions were verified before performing every experiment. The inlet velocity across the range of the cascade was found to vary less than 5% from the pitch averaged mean for all experiments. Static pressure measurements were made around the circumference of each vane at mid span and compared with predictions from a computational study. The computational study was previously performed by Thrift et al. [10] for incompressible, viscous, low-speed conditions using FLUENT [11]. Similar to that shown previously by Thrift et al. [4], the measured and predicted pressure distributions agreed indicating that the inviscid flowfield around each vane was matched to the predicted curve. In addition, mainstream temperature measurements were made in the spanwise direction and were found to never vary more than 0.75 °C from the mainstream temperature average.

Two different leakage coolant momentum flux ratios were investigated for the present study. Based on a realistic engine pressure ratio between the leakage plenum and freestream, a momentum flux ratio of $I = 2.8$ was determined. In addition, a lower momentum flux ratio more typical of that seen in the literature of $I = 0.7$ was investigated. The average momentum flux ratio was set according to Eq. (1).

$$I = \frac{MFR^2(2S)^2}{w^2} \tag{1}$$

Equation (1) indicates that the leakage coolant was also characterized by the mass flux issuing from the interface slot. A mass flux ratio (MFR) was defined as the ratio of coolant issuing from the upstream slot and entering a single passage to the mainstream mass flow rate through a single passage. The total mass flux issuing from the upstream leakage slot was measured using a laminar flow element located within the supply pipe to the slot plenum. Based on engine realistic conditions, a mass flux ratio of $MFR = 1.0\%$ was chosen for the engine realistic momentum flux ratio at $I = 2.8$.

To achieve the necessary slot coolant exit velocity to maintain $I = 2.8$ and $MFR = 1.0\%$ required a very small slot width as unlike the engine, the wind tunnel operated with a density ratio of approximately 1. Using Eq. (1), a leakage slot width of $w = 3.3$ mm was determined for the $I = 2.8$ and $MFR = 1.0\%$ condition. Consequently, the low momentum flux ratio condition at $I = 0.7$ was achieved by lowering the mass flux ratio with the given slot width to $MFR = 0.5\%$. Note that for a given momentum flux ratio the pressure ratio between the slot plenum and vane stagnation was held constant for each injection slot.

Adiabatic Effectiveness Measurements. Spatially resolved, adiabatic wall temperatures were obtained from infrared (IR) measurements of the endwall using an Inframetrics P20 IR camera. To achieve an adiabatic condition, the endwall was made of a 2.54 cm thick plate of low density closed cell polyurethane foam, which has a very low thermal conductivity (0.03 W/mK). The foam endwall was painted black to maintain a high emissivity on the endwall surface thus providing good resolution of the surface temperatures.

The test section ceiling contained 14 viewing ports, distributed across both vane passages to allow unobstructed access of the IR camera to the entire bottom endwall. At 55 cm from the bottom endwall and with an IR camera resolution of 320×240 pixels, the resulting spatial resolution at the endwall was 0.75 mm. Used for calibration, 19 type-E thermocouples were placed in the endwall surface. A set of five images were taken at each of the 14 different viewing locations during an experiment. The surface images were then post-calibrated by determining the emissivity and background temperature of the image through matching of the image temperatures with the acquired thermocouple measurements. A MATLAB program was used to assemble the individual images into a single map of the entire endwall based on the location of mutual thermocouples.

Although the thermal conductivity of the foam endwall was low, it was necessary that a small conduction correction still be used. A one-dimensional conduction correction as described by Ethridge et al. [12] was applied to all adiabatic effectiveness measurements according to the definition of η in the Nomenclature. The correction involved measuring the endwall surface effectiveness with no leakage slot and the freestream at test condition temperature. A correction value of $\eta_o = 0.1$ was measured within the vane passages. Upstream of the leakage slot, however, a correction value of $\eta_o = 0.15$ was measured because the endwall upstream of the leakage slot was made of medium density fiberboard with a higher thermal conductivity (0.13 W/m-K).

Heat Transfer Measurements. Heat transfer experiments were performed with the same methodology as adiabatic effective experiments except for two major differences. First, a constant heat flux surface was provided on the endwall in the form of a thin endwall heater. The heater was permanently bonded to a foam surface to minimize conduction losses to the external environment. The heater consisted of a serpentine inconel pattern, encapsulated in Kapton, with a thin copper layer on the flow side. Like the adiabatic surface, the heater surface was painted black to maintain a high emissivity. Second, the mainstream and coolant temperatures were both held at room temperature to ensure that the heat transfer on the surface was solely due to convection.

For all heat transfer experiments, the lowest temperature difference between the endwall thermocouples and the freestream was approximately 10 °C to minimize uncertainty in the IR measurement. Once the endwall temperatures reached a steady state value, the thermocouple data was recorded and IR images were captured according to the methodology discussed in the previous section. The percentage of the radiation heat flux loss was typically between 3–16% of the total supplied heat flux. The percentage of conduction heat flux loss was much lower in the range of 0.5–1%.

Using the measurements of adiabatic effectiveness and heat transfer a net heat flux reduction (NHFR) was calculated. The net heat flux reduction makes use of the adiabatic effectiveness and a nondimensional metal temperature, φ. As indicated in the Nomenclature, the nondimensional metal temperature accounts for the internal cooling taking place on the nonflow side of the endwall. A typical value for φ in a turbine engine is $\varphi = 0.6$ [13]. A value of $\varphi = 0.6$ was assumed for the calculation of all NHFR in the current study.

Particle Image Velocimetry Measurements. Flowfield measurements were performed in the stagnation plane of the center vane with a high-image-density, time resolved, digital particle image velocimetry (TRDPIV) system as illustrated in Fig. 2. To capture instantaneous flow structures, TRDPIV illuminates and tracks very small particles which follow the flowfield. For the current study, Di-ethylhexyl Sebacat (DEHS) seeder particles with an approximate mean diameter of 1 μm were introduced into the flow directly upstream of the wind tunnel blower using a Laskin nozzle. A dual cavity 15 W Nd:YAG laser capable of firing at 10 kHz per laser cavity was used to illuminated the tracer particles.

As shown in Fig. 2, the laser was located over the center vane. The attached optics spread the laser light into a sheet and redirected it perpendicular to the endwall and along the vane stagnation line. The illuminated particles were captured using a CMOS

camera capable of recording digital images at 2 kHz with a spatial resolution of 1024×1024 pixels. The time delay between laser pulses was adjusted for each experiment to obtain a bulk particle displacement of approximately 8 pixels. At a camera sampling frequency of 1 kHz, 3000 images were captured over 3 s for each experiment. The sampling frequency and sampling duration were chosen based on the characteristic fluid time scale, τ_f. As flowfield measurements of the HSV were being made, the characteristic fluid time scale was based on the boundary layer thickness and the freestream velocity as defined in the Nomenclature. A sampling frequency and sampling duration of 1000 Hz and 3 s corresponded to $1/12\tau_f$ and $250\tau_f$, respectively ensuring that the flow features would be temporally resolved. Time-averaged flowfields were calculated using all 3000 image pairs.

Captured images were processed using commercially available software [14]. A minimum pixel intensity background subtraction was first performed on the raw images to improve the signal-to-noise ratio. As indicated in Fig. 2, the camera was at a slight angle to the stagnation plane, typically less than 8 deg. Using the software, the adjusted raw images were corrected for the small off normal viewing angle resulting in less than a 1% correction in the axial velocities. After correction, the images were masked to remove the endwall and vane boundaries, replacing data outside the masked region with zero intensity. The images were then processed using a decreasing, multipass technique to determine the displacement vectors.

The multipass scheme employed a single pass at an interrogation window size of 32×32 pixels followed by two passes at an interrogation window size of 16×16 pixels with 50% overlap resulting in a final vector spacing of 8×8 pixels. Interrogation windows that contained at least 30% masked out area were discarded on the initial pass. For all subsequent passes an interrogation window was only discarded if at least 60% of the window was masked. The displacement vectors were calculated for each interrogation window among image pairs using a standard cross correlation, cyclic FFT-based algorithm. To improve accuracy, a fractional window offset and image mapping through bilinear interpolation was applied to each interrogation window during intermediate and final passes based on the calculated vector field in the previous pass. Vector validation was performed after each pass using a 4-pass regional median filter with adjustable criteria for the removal and re-insertion of possible spurious vectors. The vector validation scheme was visually checked for several representative instantaneous flowfields to ensure that only spurious vectors were removed.

Uncertainty Analysis. An uncertainty analysis was performed on the parameters of adiabatic effectiveness, heat transfer, and net heat flux reduction using the partial derivative method described by Moffat [15] and is presented in Table 3. For the TRDPIV velocity measurements, the uncertainty was calculated based on the average particle displacement, maximum displacement gradient, average particle image density, and signal-to-noise ratio [16,17].

High Momentum Flux Ratio Results. Fully understanding the impact of interface slot orientation on the overall cooling of the vane endwall requires investigating the reduction in heat flux provided by the injected coolant. As mentioned previously, the net heat flux reduction can be calculated from the adiabatic effectiveness and heat transfer. Figure 3 compares contours of adiabatic effectiveness for the four interface slot orientations. Although limited, injecting coolant at 90 deg with $I = 2.8$ provides some cooling to the entire endwall. An increase in the effectiveness over the entire endwall for 90 deg injection indicates that the coolant is separating and mixing with the near wall flow, creating a relatively cool layer of fluid over the entire endwall. Unfortunately, the coolant is degraded through mixing with the hot mainstream flow, leading to relatively low adiabatic effectiveness levels. For the 90 deg slot, the effectiveness of the leakage coolant is highest near the suction side leading edge. This can be attributed to the relatively low static pressure on the endwall near the suction side leading edge, increasing the local momentum and mass flux ratios.

Reducing the slot orientation angle to 65 deg provides a substantial improvement to the cooling effectiveness in comparison to the 90 deg slot. Near the pressure side of the passage where the cooling effectiveness is lowest, however, the 65 deg slot provides slightly lower effectiveness than that seen for the 90 deg slot. The adiabatic effectiveness results for 90 deg injection suggest that the coolant was able to successfully mix with the mainstream flow to such a spanwise distance as to overcome the passage vortex, allowing for some cooling at the pressure side of the passage. For the 65 deg slot, however, spanwise penetration of the coolant was reduced thus preventing the coolant from overcoming the passage vortex and cooling the pressure side of the passage.

Although a further reduction in the slot orientation angle to 45 deg does not provide an increase in the maximum effectiveness level, there is a substantial improvement in the overall spreading of high effectiveness levels in the passage. Specifically, effectiveness levels are increased at stagnation and near the pressure side of the passage, all the way to the trailing edge. The addition of a much stronger axial velocity component when the slot orientation

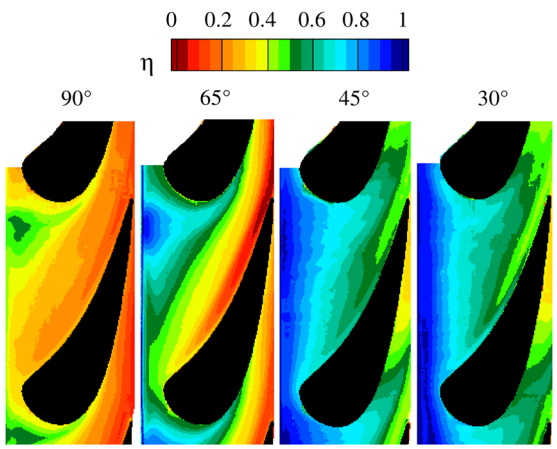

Fig. 3 Comparison of adiabatic effectiveness contours between four different slot orientations for MFR = 1.0% and I = 2.8

Table 3 Total measurement uncertainties

Measurement	Uncertainty
Adiabatic Effectiveness, η	$\partial\eta = \pm 0.025$ for $\eta = 0.03$ to 0.9
Heat Transfer, Nu	∂Nu $= \pm 6$ (2.5%) at Nu $= 250$
	∂Nu $= \pm 96$ (8%) at Nu $= 1200$
Net Heat Flux Reduction, NHFR	∂NHFR $= \pm 0.08$ (5%) at NHFR $= 1.6$
	∂NHFR $= \pm 0.06$ (20%) at NHFR $= 0.3$
Particle Image Velocimetry, U,V	$\partial U = 0.16$ m/s (2% of U_∞) for a bulk particle displacement of 8 pixels
Turbulence Intensity, Tu	∂Tu $= \pm 0.02$ for Tu $= 0.1$ to 0.4

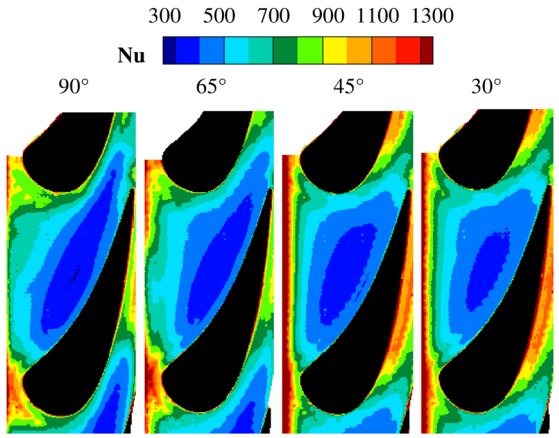

Fig. 4 Comparison of Nusselt number contours between four different slot orientations for MFR = 1.0% and I = 2.8

is reduced to 45 deg allows the coolant to penetrate further into passage. A reduction in the slot orientation to 30 deg results in a less significant change to the passage cooling effectiveness than that observed for the reduction from 65 deg to 45 deg. The injection of coolant at 30 deg, however, provides a more uniform distribution of effectiveness directly downstream of the slot.

In either case, injecting coolant at 45 deg and 30 deg allows for improved adiabatic effectiveness levels near the pressure side of the passage in comparison to the 90 deg and 65 deg slots. In combination with the improved passage pressure side cooling effectiveness the reduction in the strong sweeping of the effectiveness levels from pressure to suction side suggests that the strength of the passage vortex and endwall crossflow is diminished. Endwall crossflow is the result of the velocity deficit within the boundary layer, forcing endwall streamlines to follow a smaller radius of curvature through the passage than the freestream to maintain the balance between centripetal acceleration and the passage pressure gradient [18]. Injection along the endwall reduces crossflow by reducing the velocity deficit at the near wall, particularly just downstream of the injection slot.

Figure 4 compares contours of heat transfer in the form of Nusselt number for the four leakage slot orientations. Each slot orientation case indicates relatively low heat transfer in the endwall region near the vane pressure side. For the 90 deg and 65 deg slots, the sweeping of the low heat transfer region toward the passage throat as high heat transfer levels approach near the mid pitch of the passage supports the existence of a strong passage vortex as suggested previously from the effectiveness results. Similarly, the reduction in size and skew of the low heat transfer region for the 45 deg and 30 deg slots supports a mitigation of the passage vortex and endwall crossflow. Beyond the passage throat and along the vane suction side, however, heat transfer values are higher for the 30 deg and 45 deg slot orientations in comparison to the 90 deg and 65 deg slot orientations.

As shown in the adiabatic effectiveness results, the coolant is concentrated near the endwall just downstream of the passage throat for the 45 deg and 30 deg slots indicating little mixing with the hot mainstream flow up to that point. Beyond the passage throat, however, the effectiveness is reduced corresponding to the increase in heat transfer. The sudden reduction in effectiveness and the increase in heat transfer around the suction side indicate an increase in the near wall mixing. For the 45 deg and 30 deg slots this suggests an intensification of the passage vortex beyond the point of attachment which is typically considered to be the minimum pressure point at the passage throat.

Concerning the heat transfer near the leakage slot, the majority of the coolant for the 90 deg and 65 deg slots is concentrated near the suction side leading edge. Figure 4 indicates that the concentration of coolant near the suction side leading edge results in relatively high heat transfer in the region, particularly for the 65 deg slot where cooling effectiveness is higher. Contour results for the 45 deg and 30 deg slot orientations show a more pitchwise uniform distribution of Nusselt number downstream of the slot similar to that seen in the effectiveness results. Injecting coolant more tangential to the endwall rather than normal to the endwall where separation is likely increases the interaction of the coolant with the near wall flow at the exit of slot, providing a greater potential for heat transfer augmentation. As shown in Fig. 4, the Nusselt number values downstream of the slot near the mid pitch for the 30 deg and 45 deg slot orientations are almost twice as high as those seen for the 90 deg and 65 deg slots.

To support the observations made from the adiabatic effectiveness and heat transfer contours, Fig. 5 compares the time-averaged flowfields with overlaid streamlines and contours of turbulence intensity in the stagnation plane for the four leakage slot orientations. The stagnation of the impending boundary layer at the vane leading edge results in a pressure gradient toward the endwall as a consequence of the velocity deficit within the boundary layer. Streamlines in Fig. 5(*a*) indicate that the separated coolant injected at 90 deg is turned back to the endwall to form a leading edge vortex. The time-averaged flowfield indicates that the coolant injected at 90 deg promotes the large leading edge vortex. The presence of the vortex and the associated mixing as indicated by increased turbulence levels results in high heat transfer at the vane stagnation as shown in Fig. 4 and poor adiabatic effectiveness as shown in Fig. 3 for 90 deg injection. Also note that a small time-averaged, secondary vortex forms upstream of the injecting coolant which acts as a physical impedance to the approaching boundary layer flow similar to the vane stagnation.

Like the 90 deg slot orientation, coolant injected at 65 deg also separates from the endwall resulting in the formation of a time-averaged vortex as shown in Fig. 5(*b*). With the addition of an axial injection component and a reduced spanwise component, however, the large time-averaged vortex forms further downstream and closer to the endwall. As shown in Fig. 3, reducing the penetration depth of the coolant improves the stagnation region adiabatic effectiveness relative to the 90 deg slot. The high turbulence levels for coolant injected at 65 deg in comparison to the 90 deg slot indicate the influence of the approaching flow on the injecting coolant. Coolant injected at 90 deg acts as impedance to the incoming flow resulting in the formation of a secondary vortex. For the 65 deg slot, however, the incoming flow was able to frequently disrupt the injecting coolant. As a result of the frequent disruption the vortex formed with 65 deg injection is less steady than that observed for 90 deg injection, resulting in increased turbulence. Consequently, endwall heat transfer is also increased in the stagnation region as shown in a comparison of the 90 deg and 65 deg slots in Fig. 4. While the approaching flow does turn toward the endwall just upstream of the injecting coolant, the coolant jet was not a significant enough obstruction to result in the regular formation of a secondary vortex; thus no time-averaged secondary structure is present for 65 deg injection.

Figures 5(*c*) and 5(*d*) show that no time-averaged vortex is present in the vane stagnation plane for the 45 deg and 30 deg slot orientations. For both the 45 deg and 30 deg slot orientations, the time-averaged flowfield indicates that the coolant is injected tangential to the endwall. The injection of high velocity coolant along the endwall plane energizes the velocity deficit in the approaching boundary layer at the near wall. The stagnation of this boundary layer at the vane results in a static pressure gradient at the vane-endwall junction that is away from the endwall. Figures 5(*c*) and 5(*d*) show a strong turning of the flow toward midspan at the vane-endwall junction for both the 30 deg and 45 deg slot orientations. As shown in Fig. 4, the heat transfer close to the vane-endwall junction in the stagnation region is higher for the 90 deg and 65 deg slots than the 45 deg and 30 deg slots, respectively. The increased heat transfer near the vane stagnation in the case of the 90 deg and 65 deg slots is a result of downwash impinging on the endwall at the junction of the vane. Downwash at

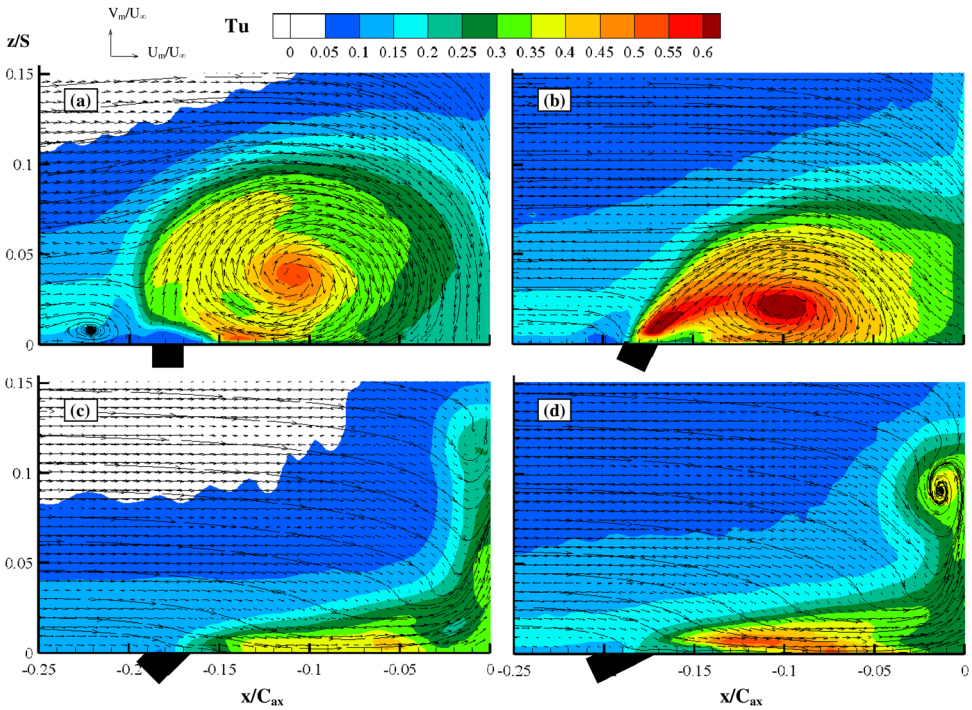

Fig. 5 Average flowfield vectors, streamlines, and contours of turbulence intensity in the stagnation plane with MFR = 1.0% and I = 2.8 for the (*a*) 90 deg, (*b*) 65 deg, (*c*) 45 deg, and (*d*) 30 deg slot orientations

the vane-endwall junction at stagnation, however, is not present for the 45 deg and 30 deg slots.

The injection of coolant along the endwall, however, does not completely fill in the velocity deficit region of the approaching boundary layer for the 45 deg and 30 deg slots. Coolant injection at 45 deg and 30 deg results in the formation of a shear layer along the interface between the high momentum coolant and the low velocity boundary layer flow. Large gradients exist in the streamwise velocity along the interface line of the shear layer causing an increase in turbulence level. The streamwise velocity gradient is stronger for coolant injected at 30 deg in comparison to the 45 deg slot because of the larger streamwise injection component; thus the turbulence levels are higher.

Streamlines in Figs. 5(*c*) and 5(*d*) indicate that the mainstream flow turns toward the endwall on approach to the vane stagnation. The interaction between the opposing flows of the coolant and mainstream at stagnation results in strong inflection points in the time-averaged streamlines. The inflection points indicate where the spanwise direction of the velocity is reversed, setting up a scenario where a counterclockwise rotating vortex can form. For the 45 deg slot, intermittent vortices are formed along the inflection points but are quickly dissipated or moved out of the stagnation plane as no vortex structure is present in the time-averaged flowfield. Stronger upwash in the case of the 30 deg slot, however, results in the regular formation of a small counterclockwise rotating vortex centered at z/S = 0.09 at the vane stagnation.

Adiabatic effectiveness and heat transfer measurements with an assumed nondimensional metal temperature can be combined to produce a net heat flux reduction to the endwall. Figure 6 compares contours of net heat flux reduction for the four slot orientations. The injection of coolant for each slot orientation provides a reduction in heat flux at every location on the endwall. A large net heat flux reduction is achieved by providing a low fluid temperature at the near wall in the presence of high heat transfer. The heat transfer contours in Fig. 4 are alike over much of the passage, excluding the region just downstream of the slot and past the passage throat. Therefore, the distribution of net heat flux reduction is most analogous to the adiabatic effectiveness distributions where

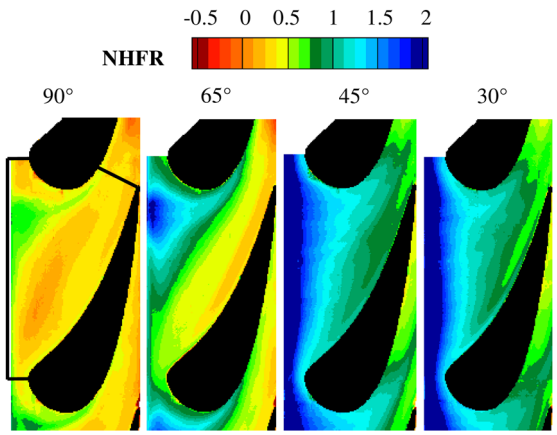

Fig. 6 Comparison of net heat flux reduction contours between four different slot orientations for MFR = 1.0% and I = 2.8

differences are larger among the different slot orientations. In addition, the reduction in heat flux is due mostly to the increase in adiabatic effectiveness associated with slot injection.

In the case of the 90 deg slot, the maximum net heat flux reduction occurs near the suction side leading edge where heat transfer and effectiveness was highest. Although reducing the slot angle to 65 deg provided only a marginal change in the endwall heat transfer, the substantial improvement in effectiveness resulted in an equally significant reduction in the net heat load experienced by the endwall. A further reduction in the injection slot angle to 45 deg does not result in as substantial of an increase in the maximum net heat flux reduction level as that seen with the injection slot orientation change from 90 deg to 65 deg. Injecting coolant at 45 deg, however, does greatly improve the net heat flux reduction in the stagnation region and near the pressure side of the passage all the way to the passage throat in comparison to the 90 deg to 65

degslots. Only a marginal change in the net heat flux reduction is observed with a reduction in slot orientation from 45 deg to 30 deg, indicating that the benefit of lowering the slot injection orientation has reached a plateau.

To quantify the improvement in heat flux associated with injecting coolant for each slot orientation, area averages of net heat flux reduction are presented in Fig. 7 for the contours presented in Fig. 6. The area over which the averages were performed extended from the downstream edge of the slot to the passage throat and across the passage pitch from one vane stagnation to the other. The averaging area is depicted in Fig. 6 on the 90 deg slot orientation contour. Figure 7 indicates that injecting coolant at 90 deg, 65 deg, 45 deg, and 30 deg results in an area average net heat flux reduction of 36%, 75%, 137%, and 131% respectively.

Low Momentum Flux Ratio Results. In addition to high momentum flux ratio experiments, results were also obtained for the injection of coolant at a lower momentum flux ratio. As mentioned previously, low momentum flux ratio experiments were performed by reducing the mass flux ratio to MFR = 0.5% thus reducing the momentum flux ratio for the fixed slot width to I = 0.7.

Figure 8 compares contours of adiabatic effectiveness for the 90 deg, 65 deg, 45 deg, and 30 deg slot orientations for the low momentum flux ratio condition. Each slot orientation indicates a strong sweeping of coolant from the pressure side to the suction side of the passage, highlighting the strong influence of the passage vortex and endwall crossflow. Unlike the I = 2.8 results, injecting coolant at I = 0.7 is insufficient in providing cooling to the endwall near the vane pressure side for each slot orientation.

Figure 8 shows that the local cooling effectiveness at the suction side leading edge is higher for the I = 0.7 case than that seen previously for the 90 deg slot with I = 2.8. Reducing the momentum flux ratio reduces the penetration depth of the coolant in to the mainstream, improving the effectiveness of the coolant near the suction side leading edge. As the local effectiveness is improved for injection at 90 deg with I = 0.7, reducing the slot orientation to 65 deg results in only a small improvement in the adiabatic effectiveness in comparison to the same orientation reduction at I = 2.8. A similar maximum cooling effectiveness level was observed for the injection of coolant at 65 deg for both the high and low momentum flux ratios. The distribution of the maximum effectiveness level, however, covered a larger region of the endwall just downstream of the slot near the suction side leading edge for injection at 65 deg with I = 0.7. Reducing the penetration depth of the coolant improves the cooling effectiveness

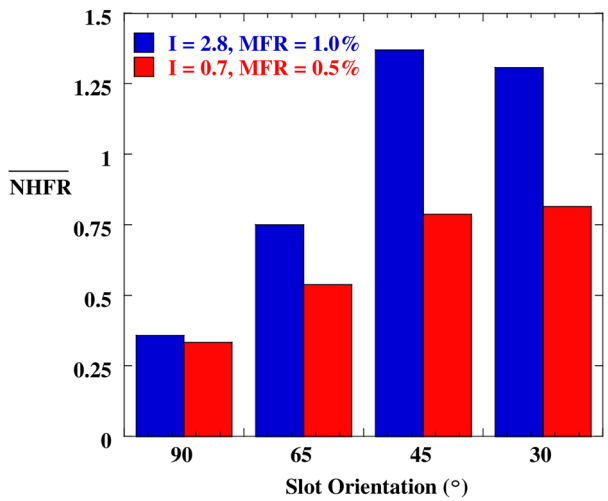

Fig. 7 Area averaged net heat flux reduction between four different slot orientations

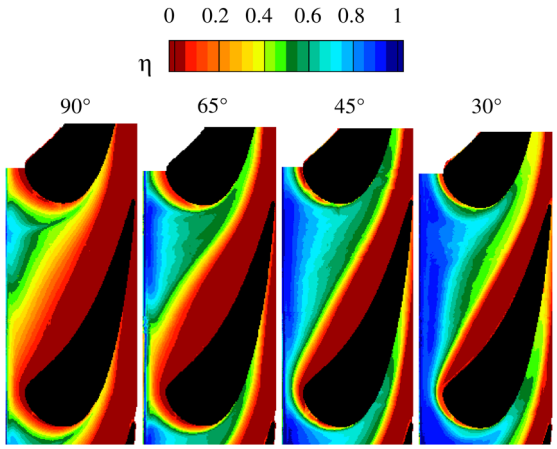

Fig. 8 Comparison of adiabatic effectiveness contours between four different slot orientations for MFR = 0.5% and I = 0.7

just downstream of the slot while the cooling effectiveness near the pressure side of the passage suffers. Reducing the slot orientation to 45 deg results in improved coolant coverage in comparison to the 90 deg and 65 deg slot orientations for low momentum injection. The overall change in effectiveness, however, is much less significant for the reduction from 65 deg to 45 deg for I = 0.7 in comparison to high momentum injection. Similar to the high momentum results, a further reduction in slot orientation to 30 deg results in only a marginal change in coolant coverage.

The overall influence of slot orientation on effectiveness is less significant at I = 0.7 than what was observed for I = 2.8. Figure 9 indicates a similar development for heat transfer in a comparison of Nusselt number contours for the four leakage slot orientations with I = 0.7. The low heat transfer region within the vane passage near the pressure side is shown to be comparable in both range and distribution between the four slot orientations as the injected coolant was unable to reach the endwall near the passage pressure side for each slot orientation. In comparison to the heat transfer results presented in Fig. 4 for the I = 2.8 condition, the minimum Nusselt number value within the passage for the low momentum flux ratio cases is shown to be approximately 10% lower. The sweeping of the low heat transfer region from pressure to suction side for each slot orientation also correlates with the sweeping of effectiveness levels indicating the strong influence of the passage vortex and endwall crossflow. Near the suction side leading edge the Nusselt number values are shown to skew toward higher values in the presence of leakage flow for each slot orientation. The

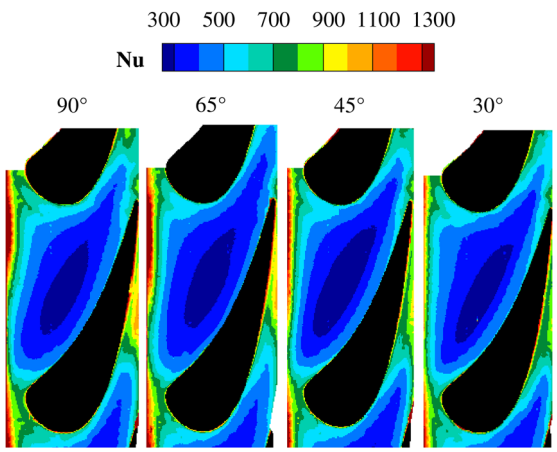

Fig. 9 Comparison of Nusselt number contours between three different slot orientations for MFR = 0.5% and I = 0.7

distribution of peak Nusselt Number values near the suction side leading edge, however, is shown to diminish in area with a reduction in the slot orientation.

At the stagnation region, Fig. 9 shows that high Nusselt number values are spread over a larger area for the 90 deg and 65 deg slots in comparison to the 45 deg and 30 deg slots. To support the stagnation region heat transfer observations, Fig. 10 presents time-averaged flowfields at the stagnation plane for all four slot orientations with I = 0.7. As shown in Fig. 10(*a*), injecting coolant at 90 deg results in the formation of a time-averaged vortex. Similar to that observed for the I = 2.8 cases, coolant injected at 65 deg results in the formation of time-averaged vortex that is slightly further downstream as a result of a reduced spanwise injection component and increased axial component. For the 45 deg and 30 deg slot orientations, however, a much smaller vortex is formed at the vane-endwall junction. In addition, the coolant interaction with the near wall flow and subsequently the turbulence levels are reduced for each reduction in slot orientation. The disparity in size and turbulence intensity of the leading edge vortex formed between the 90 deg and 65 deg slots support the wider distribution of high heat transfer in the stagnation region in comparison to the 45 deg and 30 deg slots for low momentum injection.

Compared to the flowfields shown previously in Fig. 5 for I = 2.8, the leading edge vortex that forms for coolant injected at 90 deg is much larger and results in higher turbulence levels than that seen for the low momentum flux ratio condition. For the injection of coolant at 90 deg, the leading edge vortex that forms for each momentum flux ratio case is centered at $x/C_{ax} = -0.11$. This is expected as each momentum flux ratio condition is under the influence of the same mainstream Reynolds number and boundary layer. The spanwise position of the vortex center, however, is higher for the I = 2.8 condition at z/S = 0.04 as compared to z/S = 0.02 for the low momentum flux ratio case. A higher injection velocity for the I = 2.8 case allows the coolant to penetrate further into the mainstream before being turned back to the endwall. The time-averaged vortex formed for coolant injected at I = 0.7 for the 65 deg slot also maintains the same axial location as the I = 2.8 case at $x/C_{ax} = -0.1$, In contrast to the 90 degslot, however, the vortex also maintains the same spanwise position at z/S = 0.02 for the 65 deg slot. Although the vortex location is similar between the high and low momentum flux ratio cases for the 65 deg slot, the turbulence intensity generated by the vortex is lower for the I = 0.7 case.

A comparison of the 45 deg and 30 deg slot orientation results between the two momentum flux ratio conditions in Figs. 5 and 10 show a more significant augmentation of the leading edge flowfield than that observed for coolant injection at 90 deg and 65 deg. Coolant injected at 45 deg and 30 deg with I = 2.8, flows along the endwall and is turned up at the vane-endwall junction. In reducing the momentum flux ratio to I = 0.7, however, the velocity deficit within the approaching boundary layer is not sufficiently filled in to counteract the strong turning of flow toward the endwall. As a result, a small leading edged vortex is formed at the vane-endwall junction as shown in Figs. 10(*c*) and 10(*d*). Interestingly, the similarity in stagnation plane flowfield between the 45 deg and 30 deg slot orientations is reflected in the similarity in stagnation region heat transfer for both momentum flux ratio cases, respectively. For the 90 deg and 65 deg slot orientations, only the I = 0.7 case shows strong similarities between the stagnation plane flowfield and heat transfer. At I = 2.8, the stagnation region heat transfer was higher for the 65 deg slot in comparison to the 90 deg slot, correspondingly the stagnation plane flowfields were also different with injection at 65 deg, resulting in higher turbulence levels.

For coolant injected at I = 2.8, the average coolant exit velocity is approximately 68% higher than the freestream velocity. Consequently, the large velocity difference between the injecting coolant and near wall flow leads to large separation regions for the 90 deg and 65 deg slots and strong shear layers for the 45 deg and 30 deg slots, respectively. With low momentum injection, however, the average coolant exit velocity is much closer to the freestream velocity, approximately 17% lower. The smaller velocity disparity between the injecting coolant and near wall flow for injection at I = 0.7 results in smaller separation regions and weaker shear layers, reducing the stagnation plane turbulence for each slot orientation in comparison to the respective I = 2.8 case. Expectantly, the stagnation heat transfer for coolant injection at

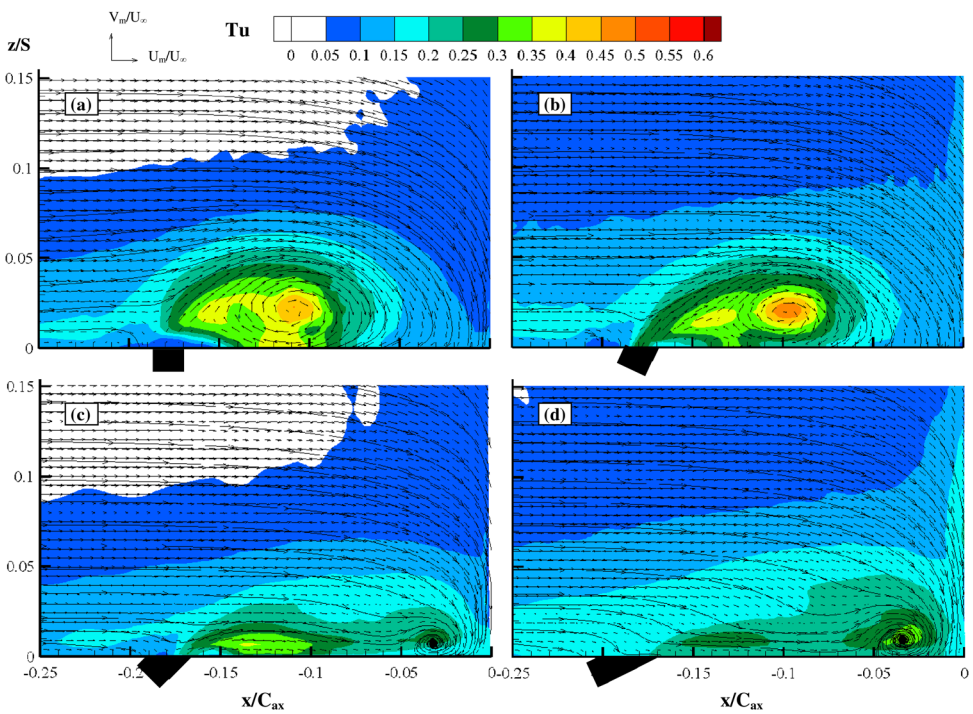

Fig. 10 Average flowfield vectors, streamlines, and contours of turbulence intensity in the stagnation plane with MFR = 0.5% and I = 0.7 for the (*a*) 90 deg, (*b*) 65 deg, (*c*) 45 deg, and (*d*) 30 deg slot orientations

I = 0.7 compared to I = 2.8 is lower for each slot orientation as shown previously in Figs. 4 and 9.

Figure 11 compares contours of net heat flux reduction between the four slot orientations for I = 0.7. A comparison of Fig. 11 to the effectiveness contours in Fig. 8 shows that the net heat flux was only reduced where coolant was present. Subsequently, the net heat flux was slightly increased on the pressure side of the passage for each slot orientation as no coolant was present. For the 90 deg slot, a reduction in momentum flux ratio from I = 2.8 to I = 0.7 results in a slight increase in peak net heat flux reduction. This is a result of the effectiveness near the suction side leading edge being higher for the I = 0.7 condition when coolant is injected at 90 deg. For the 65 deg, 45 deg, and 30 deg slot orientations, however, the peak net heat flux reduction is slightly lower between the I = 2.8 and I = 0.7 cases. Although the maximum effectiveness was similar between the high and low momentum flux cases for the 65 deg, 45 deg, and 30 deg slots, the heat transfer was much lower for the I = 0.7 cases, resulting in a reduction in peak net heat flux reduction.

The area averaged, net heat flux reduction for each slot orientation at I = 0.7 is plotted on Fig. 7 for comparison to the previously presented results at I = 2.8. Figure 7 indicates that injecting coolant at 90 deg, 65 deg, 45 deg, and 30 deg results in an area average net heat flux reduction of 33%, 54%, 79%, and 81%, respectively. Reducing the momentum flux ratio from I = 2.8 to I = 0.7 results in a percent difference reduction in area averaged heat flux reduction of 8%, 28%, 42%, and 38% for the 90 deg, 65 deg, 45 deg, and 30 deg slot orientations, respectively. The average net heat flux reduction is much lower for the I = 0.7 results in comparison to the I = 2.8 results for several reasons. The first is related to the reduction in coolant mass flow from MFR = 1.0%, to MFR = 0.5% for the lower momentum flux ratio case. Recall that the momentum flux ratio was reduced by reducing the MFR of the coolant through the fixed slot width. As shown in previous studies [3,19,20], the effect of lowering the coolant mass flux ratio is to reduce the spreading of high effectiveness values within the passage while only marginally altering the maximum effectiveness value. Second, the endwall heat transfer is higher for high momentum injection in comparison to low momentum injection for each respective slot orientation. Reduced effectiveness levels and lower heat transfer within the passage for injection at I = 0.7 compared to I = 2.8 combines to produce lower area averaged, net heat flux reduction.

Reducing the slot orientation is shown to increase the average net heat flux reduction by a greater extent for the high momentum flux ratio condition. For coolant injected at I = 0.7, reducing the slot orientation results in a fairly linear increase in area averaged net heat flux down to a slot orientation of 45 deg, below which the results plateau. For high momentum injection, however, an exponential increase in area averaged net heat flux reduction is observed down to a slot orientation of 45 deg. As discussed previously, a fundamental difference in the endwall adiabatic effectiveness, heat transfer, and stagnation plane flowfields exists between the 90 deg and 65 deg slots and the 45 deg and 30 deg slots, respectively, at I = 2.8. For low momentum injection, however, thermal and velocity field measurements indicate fewer differences among the four slot orientations.

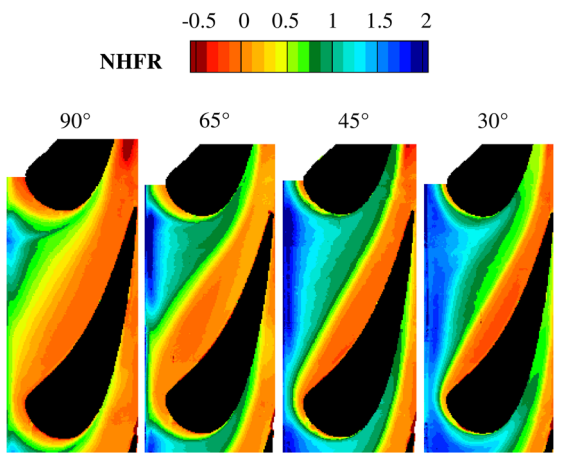

Fig. 11 Comparison of net heat flux reduction contours between four different slot orientations for MFR = 0.5% and I = 0.7

Conclusions

Thermal and velocity measurements were performed in a nozzle guide vane passage to investigate the cooling performance of a 90 deg, 65 deg, 45 deg, and 30 deg interface slot orientation. Two leakage flow conditions were considered, an engine realistic momentum ratio and a low momentum flux ratio.

Coolant injected at the engine realistic momentum flux ratio provided some cooling effectiveness to the entire endwall for each slot orientation. Systematically reducing the slot orientation was shown to improve cooling effectiveness and coverage uniformity, particularly near the pressure side of the passage and trailing edge down to a slot orientation of 45 deg. A final reduction in slot orientation to 30 deg did not provide any substantial improvement over coolant injected at 45 deg. The absence of a strong sweeping in the effectiveness values from the pressure side to the suction side of the passage for the 45 deg and 30 deg slots indicated that the passage vortex and endwall crossflow were diminished. Simultaneously lowering the momentum and mass flux ratio restricted the injected coolant to the suction side of the passage indicating the strong influence of secondary flows for each slot orientation.

Similar to the adiabatic effectiveness results, heat transfer patterns were shown to be characteristically different between the 90 deg and 65 deg slots and the corresponding 45 deg and 30 deg orientations at the engine realistic momentum flux ratio. For the 90 deg and 65 deg orientations, the highest heat transfer occurred in the stagnation region. A leading edge, time-averaged vortex was formed in the stagnation plane when coolant was injected at both 90 deg and 65 deg, considerably augmenting the local turbulence and endwall heat transfer. For coolant injected at 45 deg or 30 deg, no large time-averaged vortex was present; instead, a strong upwash of fluid at the vane-endwall junction was observed. Injecting coolant along the plane of the endwall produced strong shear layers and subsequently high turbulence levels at the endwall directly downstream of the slot. As a result, very high heat transfer values were observed downstream of the interface slot along the entire passage pitch instead of just at the stagnation region. Reducing the momentum flux ratio reduced the velocity difference between the injecting coolant and near wall flow, substantially reducing the mixing and the resulting turbulence levels. Subsequently, endwall heat transfer levels were reduced for each slot orientation. Although weaker in intensity, a time-averaged vortex was still formed in the stagnation plane for both the 90 deg and 65 deg slot orientations at low momentum injection. For the 45 deg and 30 deg slot orientations, the injection of low momentum coolant was insufficient in counteracting the strong turning of flow toward the endwall leading to the formation of a small vortex at the vane-endwall junction.

Injecting coolant at the engine realistic momentum flux ratio reduced the net heat flux to the endwall at each point within the vane passage for all four slot orientations. Reducing the interface slot orientation, however, significantly improved the overall reduction in net heat flux with area averaged, net heat flux reductions as high as 137%. In combination with lower endwall heat transfer owing to reduced turbulence levels, the absence of coolant near the pressure side of the passage resulted in lower area averaged net heat flux reduction for the reduced momentum and mass flux ratio cases. While reducing the interface slot orientation for low momentum injection improved the net heat flux reduction, the highest area average was lower than for higher momentum injection at only 80%.

Although an angled slot is more complex than a perpendicular slot, the substantial improvement in endwall cooling provided by reducing the slot orientation may outweigh the possible complexities associated with an angled interface. The current paper has shown that injecting coolant at a high momentum flux ratio of $I = 2.8$ and $MFR = 1.0\%$ with an orientation of 45 deg would provide the largest reduction in heat load to the vane endwall.

Acknowledgment

The authors wish to thank Mitsubishi Heavy Industries LTD for their support of this work, specifically Mr. Tsukagoshi and Mr. Masada for their technical advice.

Nomenclature

- C = true vane chord
- h = heat transfer coefficient
- I = momentum flux ratio
- Ma = Mach number
- MFR = leakage mass flux ratio
- $NHFR$ = net heat flux reduction, $(q''_o - q''_c)/q''_o = 1 - h_c/h_o(1 - \eta/\varphi)$
- Nu = Nusselt number, $q''_{conv}C_{ax}/(T_w - T_\infty)k_{air}$
- P = vane pitch
- q'' = heat flux
- Re = Reynolds number, UC/ν_{air}
- S = vane mid span height
- T = static temperature
- Tu = turbulence intensity, $(u^2_{rms} + v^2_{rms})^{1/2}/U_\infty$
- U = instantaneous streamwise velocity
- V = instantaneous spanwise velocity
- w = slot width
- x = axial direction
- y = pitch direction
- z = span direction

Greek Symbols

- α = flow angle
- δ = boundary layer thickness
- δ^* = displacement thickness
- η = corrected adiabatic effectiveness, $(\eta_{exp} - \eta_o)/(1 - \eta_o)$
- η_{exp} = measured adiabatic effectiveness, $(T_\infty - T_{aw})/(T_\infty - T_c)$
- θ = momentum thickness
- φ = nondimensional metal temperature $(T_\infty - T_w)/(T_\infty - T_{c,internal})$
- ρ = air density
- τ_f = characteristic fluid time scale, (δ/U_∞)
- ν = kinematic viscosity

Subscripts

- aw = adiabatic wall
- ax = axial chord
- c = coolant
- $conv$ = heat transfer through convection
- $exit$ = exit of vane passage at throat
- in = measured at inlet of the vane cascade
- m = time-averaged measurement
- o = no coolant
- w = wall
- ∞ = freestream condition at the entrance to the test section
- θ = based on momentum thickness

References

[1] Lin, Y.-L., Shih, T. I.-P., Chyu, M. K., and Bunker, R. S., 2000, "Effects of Gap Leakage on Fluid Flow in a Contoured Turbine Nozzle Guide Vane," ASME Paper No. GT2000-0555.

[2] Rehder, H. J., and Dannhauer, A., 2007, "Experimental Investigation of Turbine Leakage Flows on the Three-Dimensional Flow Field and Endwall Heat Transfer," J. Turbomach.,**129**, pp. 608–618.

[3] Thrift, A. A., Thole, K. A., and Hada, S., 2011, "Effects of Orientation and Position of the Combustor-Turbine Interface on the Cooling of a Vane Endwall," ASME Paper No. GT2011-45507.

[4] Sundaram, N., and Thole, K. A., 2009, "Film-Cooling Flowfields With Trenched Holes on an Endwall," J. Turbomach., **131**, p. 041007.

[5] Radomsky, R. W., and Thole, K. A., 2000, "High Freestream Turbulence Effects on Endwall Heat Transfer for a Gas Turbine Stator Vane," J. Turbomach., **122**, pp. 699–708.

[6] Thole, K. A., Radomsky, R. W., Kang, M. B., and Kohli, A., 2002, "Elevated Freestream Turbulence Effects on Heat Transfer for a Gas Turbine Vane," Int. J. Heat Mass Transfer, **23**, pp. 137–147.

[7] Ames, F. E., Barbot, P. A., and Wang, C., 2003, "Effects of Aeroderivative Combustor Turbulence on Endwall Heat Transfer Distributions Acquired in a Linear Vane Cascade," J. Turbomach., **125**, pp. 210–220.

[8] Nix, A. C., Diller, T. E., and Ng, W. F., 2007, "Experimental Measurements and Modeling of the Effects of Large-Scale Freestream Turbulence on Heat Transfer," J. Turbomach., **129**, pp. 542–550.

[9] Thrift, A. A., Thole, K. A., and Hada, S., 2010, "Effects of a Sloped Endwall on a Nozzle Guide Vane: Adiabatic Effectiveness Measurements," J. Turbomach., **133**, p. 4002965.

[10] Thrift, A. A., Thole, K. A., and Hada, S., 2010, "Effects of an Axisymmetric Contoured Endwall on a Nozzle Guide Vane: Convective Heat Transfer Measurements," J. Turbomach., **133**, p. 4002966.

[11] Fluent Inc., 2006, FLUENT (version 6.2.1), Fluent Inc., Lebanon, NH

[12] Ethridge, M. I., Cutbirth, J. M., and Bogard, D. G., 2000, "Scaling of Performance for Varying Density Ratio Coolants on an Airfoil With Strong Curvature and Pressure Gradients," J. Turbomach., **123**, pp. 231–237.

[13] Bogard, D. G., *The Gas Turbine Handbook*, National Energy Technology Laboratory, Pittsburg, PA, Chap. 4.2.2.1.

[14] LaVision, 2008, "Product-Manual for *Davis* 7.2," LaVision GmbH, Gottingen, Germany.

[15] Moffat, R. J., 1988, "Describing the Uncertainties in Experimental Results," Exp. Therm. Fluid Sci., **1**, pp. 3–17.

[16] Raffel, M., Willer, C., Wereley, S., and Kompenhans, J., 1998, *Particle Image Velocimetry: A Practical Guide*, Springer, New York.

[17] Scarano, F., and Riethmuller, M. L., 2000, "Advances in Iterative Multigrid PIV Image Processing," Exp. Fluids, **29**, pp. S51–S60.

[18] Thole, K. A., *The Gas Turbine Handbook*, National Energy Technology Laboratory, Pittsburg, PA, Chap. 4.2.3.

[19] Lynch, S. P., and Thole, K. A., 2008, "The Effect of Combustor-Turbine Interface Gap Leakage on the Endwall Heat Transfer for a Nozzle Guide Vane," J. Turbomach., **130**, p. 041019.

[20] Cardwell, N. D., Sundaram, N., and Thole, K. A., 2007, "The Effects of Varying the Combustor-Turbine Gap," J. Turbomach., **129**, pp. 756–764.